




Article

Failure Characterization and Analysis of a Sport Utility Vehicles SUV Rear Door Damper Made by Nylon as Structural Element

Jorge Cruz-Salinas ¹, Pedro Jacinto Paramo-Kañetas ², Gonzalo Valdovinos-Chacón ³,
Néstor Efrén Méndez Lozano ^{1,*} , Marco Antonio Zamora-Antuñano ^{1,*}  and Sergio Arturo Gama-Lara ^{3,*} 

¹ Engineering Department, CIIDETEC-Querétaro, Universidad del Valle de México, Querétaro 76230, Mexico; j.cruz@inteligenciacolectivakm.com (J.C.-S.); nestor.mendez@uvmnet.edu (N.E.M.L.)

² Engineering Department, CIIDETEC-Coyoacán, Universidad del Valle de México, Coyoacán 04910, Mexico; pedro.paramo@uvmnet.edu

³ Engineering Department, CIIDETEC-Toluca, Universidad del Valle de México, Toluca 52164, Mexico; gonzalo.valdovinosch@uvmnet.edu

* Correspondence: marco.zamora@uvmnet.edu (M.A.Z.-A.); sergio.gama@uvmnet.edu (S.A.G.-L.); Tel.: +52-4421905214 (M.A.Z.-A.); +52-7221694529 (S.A.G.-L.)

Abstract: In this investigation, an automotive component made of nylon as a structural element was studied by several characterization techniques to identify material properties. Firstly, a Fourier transform infrared spectroscopy (FTIR) was carried out to obtain information about composition, then, differential scanning calorimetry (DSC) was used to extract useful information on sample thermal behavior. The humidity and volatile materials percentage could be assessed by thermogravimetry analysis (TGA). Morphology and topography were carried out by optical microscopy, moreover, X-ray Tomography allows it to display the sample's inner part. Characterization shows that the component could have been contaminated or exposed to conditions that promote degradation after the manufacturing process. Finally, computerized X-ray tomography displayed that both samples showed a difference in porosity in a fractured sample and a healthy sample. All the above implies a change in the mechanical integrity of the fractured material but might not omit the fact that it could have been subjected to any type of impact or mechanical effort.

Keywords: biodegradation; failure analysis; crystallinity degree; thermal characterization; car rear door damper



Citation: Cruz-Salinas, J.; Paramo-Kañetas, P.J.; Valdovinos-Chacón, G.; Lozano, N.E.M.; Zamora-Antuñano, M.A.; Gama-Lara, S.A. Failure Characterization and Analysis of a Sport Utility Vehicles SUV Rear Door Damper Made by Nylon as Structural Element. *Processes* **2023**, *11*, 1885. <https://doi.org/10.3390/pr11071885>

Academic Editors: Lin Feng Ng, Chandrasekar Muthukumar and Ruey Shan Chen

Received: 6 May 2023

Revised: 17 June 2023

Accepted: 19 June 2023

Published: 23 June 2023



Copyright: © 2023 by the authors. Licensee MDPI, Basel, Switzerland. This article is an open access article distributed under the terms and conditions of the Creative Commons Attribution (CC BY) license (<https://creativecommons.org/licenses/by/4.0/>).

1. Introduction

For some time now, automotive component stress analysis has been developed and has recently been systematized based on new evaluation techniques. Component failure has been studied in many different ways before (and will be mentioned in this document). Critically it has been found that component quality is dependent on the manufacturing process to avoid breakages, brittle components, or surface flaws, and in turn, it has been shown that the physical, chemical, and mechanical properties of some polymers are essential elements of a components' quality control. This work aims to analyze the support failure for a car rear door damper made from nylon as its main element, applying several characterization techniques to determine the cause of failure.

Nylon 6,6 is a synthetic polymer often used to produce fibers for many industrial applications. Properties of nylon can be varied by mixing it with different additives. It stands out from other polymers because of its high toughness and resistance to shock, fatigue, and low temperatures [1]. Characteristics of this material for engineering industrial plastics are ideal mainly because of its wear resistance; it is compact, hard, with good flexibility and machinability [2]. Some results showed that the addition of some nanoparticles of polyaniline and ZnO of each component to nylon-6,6 improve its antibacterial properties [3]. Furthermore, adding glass fiber to nylon-6,6 has been shown

to significantly improve its mechanical properties, such as tensile strength and elastic modulus [4]. Polyamides such as nylon present a high resistance to biodegradation, principally due to the symmetry in their molecular structures and their intermolecular hydrogen bonds; this makes nylon widely used because of its high tensile strength and resulting in a crystalline morphology with great mechanical and thermal properties. Similarly, the polyamide characteristics, such as its intermolecular cohesive force derived from the hydrogen bonds, lower the abiotic degradation speed in comparison to the accumulating one in the environment. For this reason, it becomes a priority to propose some degradation processes with faster rates contrary to the accumulating ones [5]. Degradation of these components through a chemical procedure has already been proposed in two different ways: with solvents or through thermal contact [6,7].

As mentioned above, some studies have focused on the mechanical and thermal characterization of nylon as the main element or when doped with other elements. For example, according to Polat et al. [8], the use of nylon nanofibers doped with graphene increased the fatigue life cycle as a jointing composite element. Alternatively, Kim et al. [9] prepared mixtures of polyphenylene ether and nylon with high mechanical hardness and a flame-retardant material. These studies showed that doped nylon increased its mechanical properties. Further, Zang et al. [10] characterized the physicochemical properties of nylon fibers doped with permanganate ions to measure their antibacterial capability and mechanical properties. However, as mentioned before, nylon degradation is an aspect that must be taken into consideration during the characterization; for instance, solvent, thermal, or even degradation caused by micro-organisms represent an essential factor to be analyzed.

An indirect method to determine any of the mentioned types of degradation is to potentialize the growth of the micro-organisms in a proper medium while using nylon fiber as the only carbon source. Several researchers have demonstrated that some micro-organisms can degrade the nylon-6, such as the white rot fungus, *phanerochaete chrysosporium*, and *Trametes versicolor* decompose the membrane of nylon-6 and the nylon-6,6. Thus, Deguchi et al. [11,12] found that white rot fungus strain IZU-154 degrades the nylon-6,6 membrane in 20 days, and the addition of manganese accelerates the degradation activity, suggesting that ligninolytic enzymes are involved. Subsequently, Friedrich et al. [13] notified that two ligninolytic fungi of white rot were responsible for the nylon-6 degradation. These fungi were *P. chrysosporium*, mainly known as a ligninolytic fungus, and *Bjerkandera adusta*, which showed a higher capability for decomposing nylon-6. The *P. chrysosporium* was described previously by Klun et al. [14], who demonstrated that molecular mass was reduced by 50% after exposing the fungus for 3 months.

Additionally, Sudhakar et al. [5] investigated some fungi that were isolated from nylon-6 samples in a factory because none of them was able to decompose the fiber. It was shown that a marine bacterium could decompose nylon-6 and nylon-6,6, for example: *Bacillus cereus*, *Bacillus spherical*, *Vibrio furnissi*, and *Brevundimonas versicular* come from the Indian Ocean. These bacteria grew up among mineral salts and showed the use of carbon and nitrogen from nylon-6/nylon-6,6 as their main carbon and nitrogen source.

Bearing the above in mind, several characterization techniques used in the current investigation have been used before in polymer compounds and polyamides, in order to measure crystallinity, thermal and mechanical properties, humidity, and glass transition. For instance, Xie et al. used differential scanning calorimetry (DSC) [15] to measure the thermal conductivity of three different types of nylon after going through complete recrystallization, finding that thermal conductivities had a higher thermal conductivity due to hydrogen bonds' major density. Sambale et al. [16] determined the polyamide's humidity gradients while measuring the glass transition by also using the DSC step scanning analysis. Recently, Patti et al. [17] conducted a comparative study of the "Basoalto' fibers" thermal properties against the traditional glass fibers in composite elements with a polyamide basis, whereby using the DSC with which the glass transition temperature (Tg), the fusion

temperature atmosphere, the enthalpy fusion (ΔH_f), and the degree of crystallinity (X_c) were measured.

The infrared spectroscopy used by Shinzawa et al. [18] was an optical characterization technique based on the combination of a near-infrared spectrometer (NIR) and a nylon tensile strength-testing machine. The analysis suggests the presence of polymer structures that experience different variations during the tension lengthening induces the orientation, and consequently, the following lengthening to create an elastic deformation.

Oshiro et al. [19] measured the nylon-6 films spectrums by using the Stark-effect infrared technique in a band of amides, while Cernohorský et al. [20] measured the spectrums of the PA6 materials and the polyvinylidene (PVDF)/PA6 mixture throughout the Fourier transform infrared spectroscopy (FT-IR) to be able to compare them with the pure polyvinylidene material (PVDF) while combining the polyvinylidene fluoride nanofibers during the spinning process. Recently, Lim et al. [21] manufactured graphite nanosheets (nylon-610) and nanocomposites to which infrared spectroscopy was made through a Fourier transform (FTIR) so an analysis of different functional groups and chemical bonds inside the nanosheets could be achieved.

Thermogravimetry (TGA) was analyzed by Lima et al. [22], who evaluated the creep of flexible polyamide flowlines to determine quantities of plasticizers in operation. Moreover, Luna et al. [23] mixed some nanocomposites made of nylon-6 acrylonitrile–butadiene–styrene in a molten state during which the nylon-6 showed thermal stability superior to high temperatures and mixtures, while nanocomposites displayed intermediate thermal decomposition behavior in comparison to pure components.

The X-ray tomography studied by Baranowski et al. [24] measured the polymer components local fiber orientation using a computerized X-ray tomography where the 3D fibers with a diameter less than a voxel could be examined. In addition, Liebrich et al. [25] explored porosity distribution on thin polymer sheets sintered with laser via X-ray microphotography, where experimental evidence was found that proves that porosity on the thin sheets depends largely upon the thickness and orientation during its construction. Lately, Butenegro et al. [26] developed new thermoplastic components out of the waste of rods made of epoxy compounds reinforced with carbon fiber, whose characterization was carried out by X-ray microphotography to examine the fibers distribution within the compounds.

2. Materials and Methods

Three samples were received; one “healthy sample”, one naturally “fractured sample”, and the last one intentionally fractured (for microscopy). During the materials characterization procedure, several techniques were applied through which contrasting information came out for each one of the samples. Firstly, a Fourier transform infrared spectroscopy (FTIR) was carried out in order to obtain information about composition samples while setting a measuring range of $4000\text{--}720\text{ cm}^{-1}$ and a resolution range of 4 cm^{-1} in an infrared spectrometry model 640-IR of Agilent Technologies (Santa Clara, CA, USA) equipped with an ATR accessory and a Ge crystal.

Differential scanning calorimetry (DSC) was carried out with a Q2000 model TA Instruments branded (New Castle, DE, USA) calorimeter under nitrogen atmosphere-proof conditions, according to the ASTM D3418 standard [27]. In terms of thermal conditions, it went from $40\text{ }^{\circ}\text{C}$ to $300\text{ }^{\circ}\text{C}$, then it cooled from 300 to $-10\text{ }^{\circ}\text{C}$ at a speed of $10\text{ }^{\circ}\text{C}/\text{min}$, with an isotherm within 5 min at $-10\text{ }^{\circ}\text{C}$, finishing with a second heating of -10 to $300\text{ }^{\circ}\text{C}$ at a speed of $10\text{ }^{\circ}\text{C}/\text{min}$, as well. The sample weight was between 3 to 5 mg taking into consideration that the reference weight was 52.81 mg ; both of them were put on a Tzero aluminum platter, and this technique was used to extract useful information regarding sample thermal behavior. For this purpose, the humidity and volatile materials percentage can be known by using the thermogravimetry analysis (TGA) with a Q50 model TA Instruments branded analyzer with a heat of 40 to $600\text{ }^{\circ}\text{C}$ at a speed of $10\text{ }^{\circ}\text{C}/\text{min}$ in an N_2 atmosphere and from 600 to $650\text{ }^{\circ}\text{C}$ under an O_2 atmosphere,

considering a sample weight range between 15 and 20 mg. It can be observed that the morphology and topography of samples through optical microscopy were carried out in an AXIO Zoom V16 model Carl Zeiss branded (Jena, Germany) stereoscopic optical microscope at different magnifications, although the X-ray computed tomography (XCT) allows it to display the sample's inner part. X-ray computed tomography was carried out in a ZEISS METROTOM Computed Tomography System with GOM Volume Inspect analysis software for 3D Computed Tomography (CT) with a voxel size of $65.3\ \mu\text{m}$, measuring a volume of $165 \times 140\ \text{mm}$ and a pixel size of $78 \times 78\ \mu\text{m}$.

3. Results

Due to the nature of nylon, the degradation process is not easy to determine, the reason that Fourier transform infrared spectroscopy (FT-IR) and DSC base their analysis methodology mainly on observations of nylon fiber structure. Another method used to evaluate the biodegrading process is one where micro-organisms growth in nylon is determined as the only carbon source.

3.1. FTIR

Figure 1 shows a comparison between the spectra where similarities between them can be appreciated; the significant absorption bands that could lead to identifying the presence of any other component cannot be observed. The spectra show peaks at $3300\ \text{cm}^{-1}$ (-NH stretching), $2933\ \text{cm}^{-1}$, $2860\ \text{cm}^{-1}$ (C-H stretching bands), $1638\ \text{cm}^{-1}$ (amide I), $1540\ \text{cm}^{-1}$ (amide II), $1418\ \text{cm}^{-1}$ (deformation C-H), and $1371\ \text{cm}^{-1}$ (deformation N-H, C-H) [28,29] as the characteristic bands found in the nylon-6,6 spectra. Nylon-6,6 has characteristics peaks for amorphous ($1138\ \text{cm}^{-1}$) and crystalline ($935\ \text{cm}^{-1}$) regions, and between the amorphous and crystalline regions, a transition region is found, indicating a semi-crystalline material [29–31]. Figure 1 shows an increase in the intensity of the transition region peak and a decrease in the crystalline region peak in the fractured material compared to the healthy material. Furthermore, the fractured material has a lower peak intensity at $3300\ \text{cm}^{-1}$ (-NH stretching) and $935\ \text{cm}^{-1}$ (crystalline peak) compared to the healthy material. Characteristic peaks for the crystalline and amorphous region shifted from 934.7 to $935.7\ \text{cm}^{-1}$ and 1114.3 to $1120\ \text{cm}^{-1}$, respectively. All this indicates that the fractured material has a lower percentage of crystallinity. The peak at $1020\ \text{cm}^{-1}$ is the absorption peak attributed to Si-O-Si groups, which are characteristics of glass fiber [32]. The analysis does not indicate a contrast among the chemical bonds in the sample, so while searching library spectra as shown in Figure 2, the major similarities were between polyamide nylon-6,6 and glass fiber, these being two the materials which were elaborated on according to the given information by the client.

3.2. Differential Scanning Calorimetry

Figure 3 presents thermograms of the first heating cycle, and Figure 4 presents thermograms of cooling and the second heating cycle of the healthy and fractured material showing a melting process between $254.15\ ^\circ\text{C}$ for both samples, which is certainly up to that reported for nylon-6,6 (melting temperature: 254 to $264\ ^\circ\text{C}$) [33]. The minimum crystallization temperature for a non-fractured material is $224.97\ ^\circ\text{C}$ (Figure 3a) and for the fractured material is $225\ ^\circ\text{C}$ (Figure 3b), supporting that polymer material in both cases is similar. Crystallinity percentages were calculated in situ by a differential scanning calorimetry (DSC) machine, following the ASTM D3418 standard [27] and the percentage of 100% crystalline nylon-6.6. If the percentage of crystallinity is calculated, taking $226\ \text{J/g}$ as a reference for 100% crystalline nylon-6.6 [34], then the healthy material has an initial crystallinity percentage of 15.39% ($34.79\ \text{J/g}$; see Figure 3a) and can form under cooling conditions, at 14.30% ($32.32\ \text{J/g}$; see Figure 4a) crystallinity, while in the piece of material with fractures, the percentages were 14.57% ($32.93\ \text{J/g}$; see Figure 3b) and 13.51% ($30.54\ \text{J/g}$; see Figure 4b), respectively.

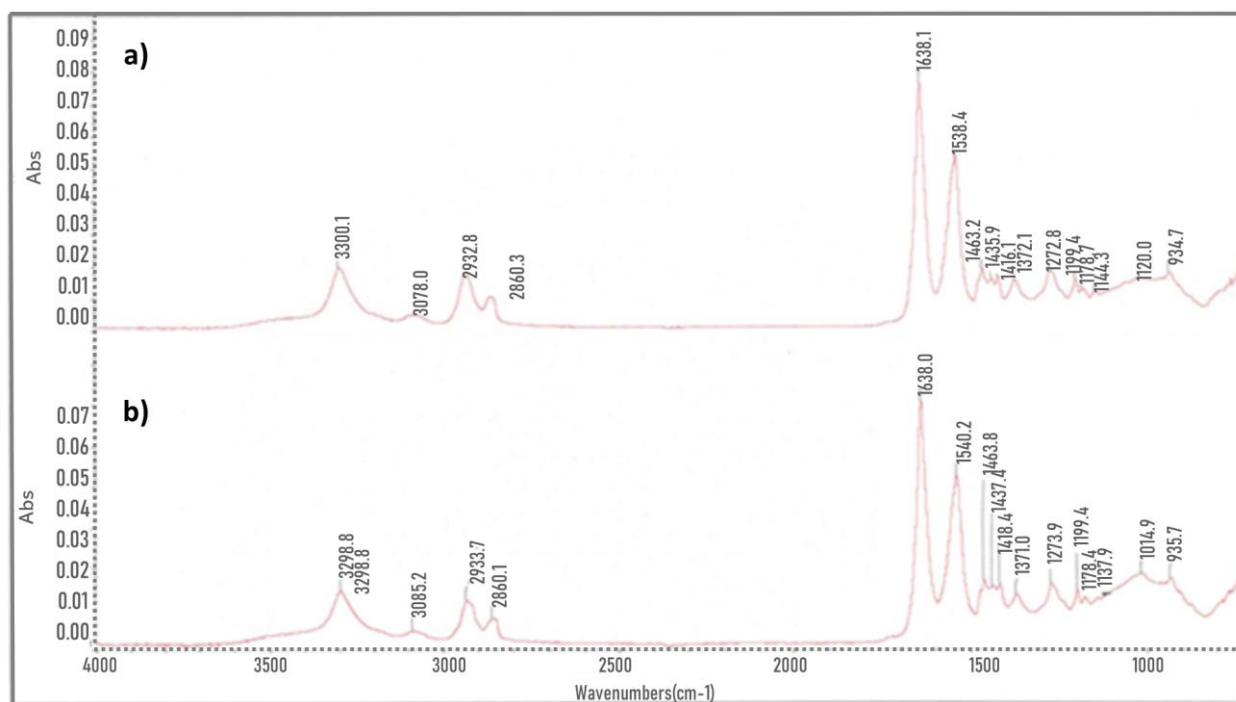


Figure 1. FTIR spectra of sample 7175 NH (a) healthy material and (b) fractured material.

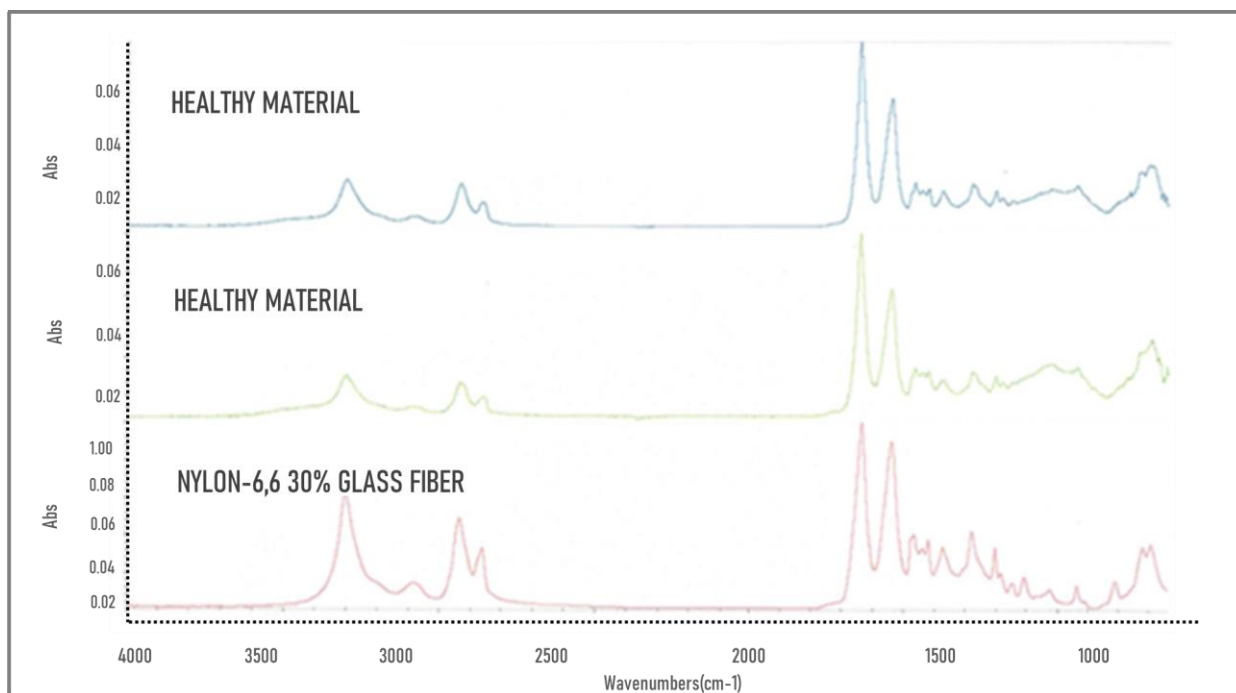


Figure 2. FTIR spectra of sample 7175 NH healthy material, 7175 NH fractured material, and vs. nylon-6,6 30% glass fiber library spectra.

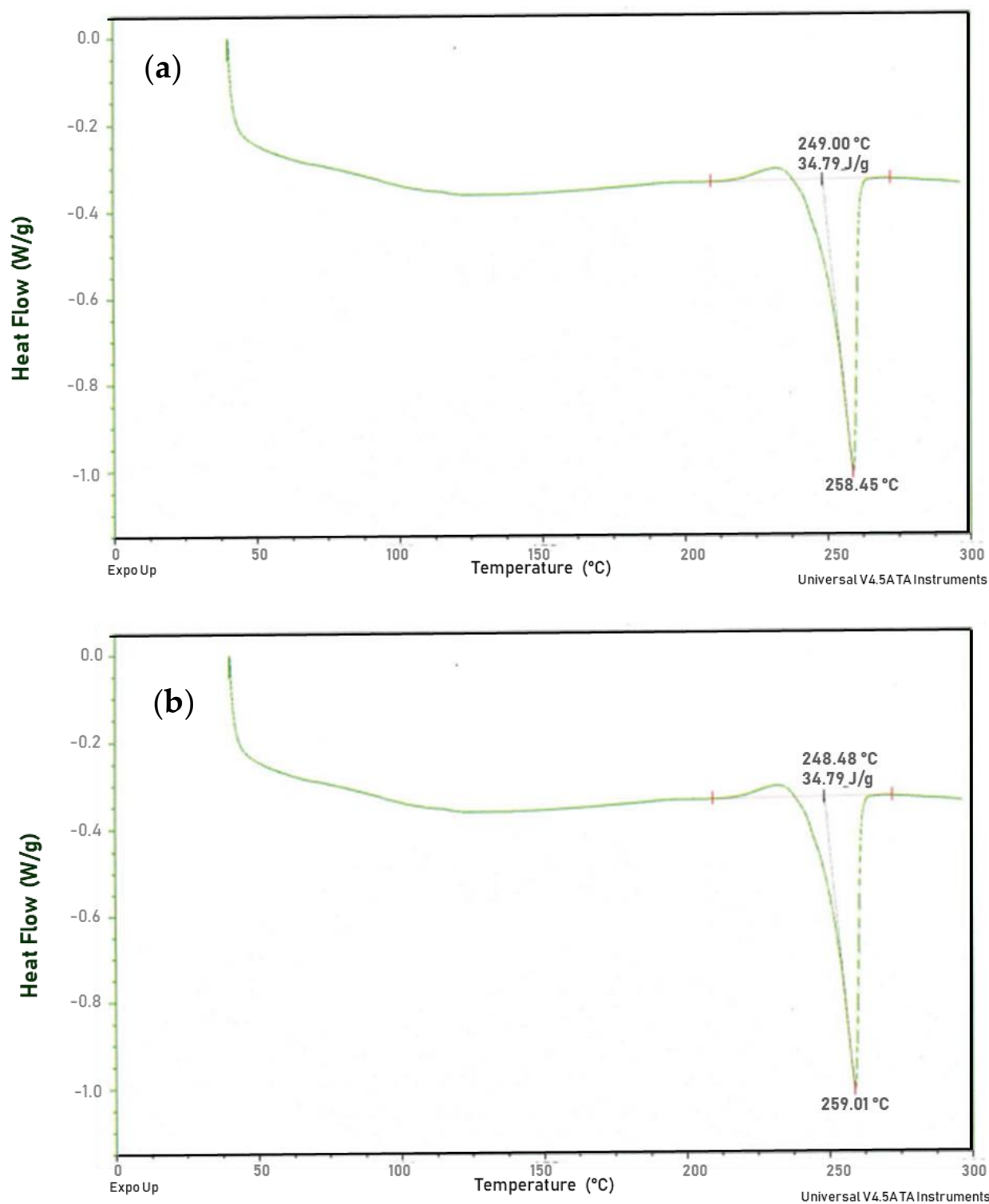


Figure 3. Thermograms of the first heating cycle of sample 7175 NH (a) healthy material and (b) fractured material.

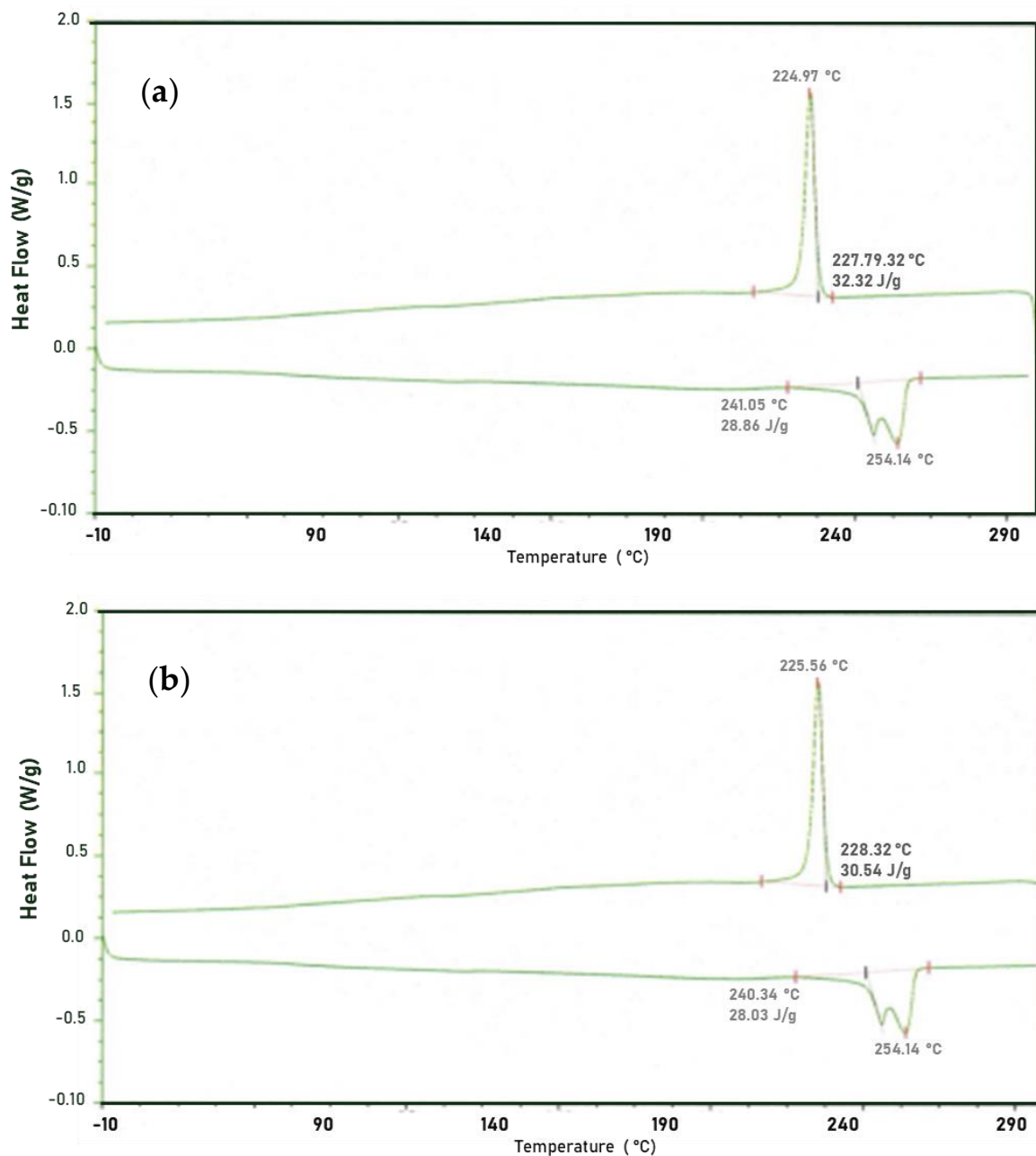


Figure 4. Thermograms of the cooling and the second heating cycle of sample 7175 NH (a) healthy material and (b) fractured material.

3.3. Thermogravimetry Scanning

To perform this analysis, a major failure zone sample was taken, and likewise, in the non-fractured material, the equivalent zone was selected. The thermograms that were obtained for samples are shown in Figure 5, displaying some relevant differences between the samples. The summary of results is depicted in Table 1, as follows: the weight loss in the range of 40–300 °C is attributable to the humidity, as well as to a volatile organic compound and low molecular weight; the second located loss is between 300 and 600 °C, which is attributable to polymer material decomposition; and the third weight loss caused by the atmosphere changes around the sample above 600 °C, is directly associated with the presence of carbonaceous materials that guarantee the total sample decomposition and, therefore, the presence of inorganic waste above 650 °C, which according to given information by the client consists mainly of fiberglass.

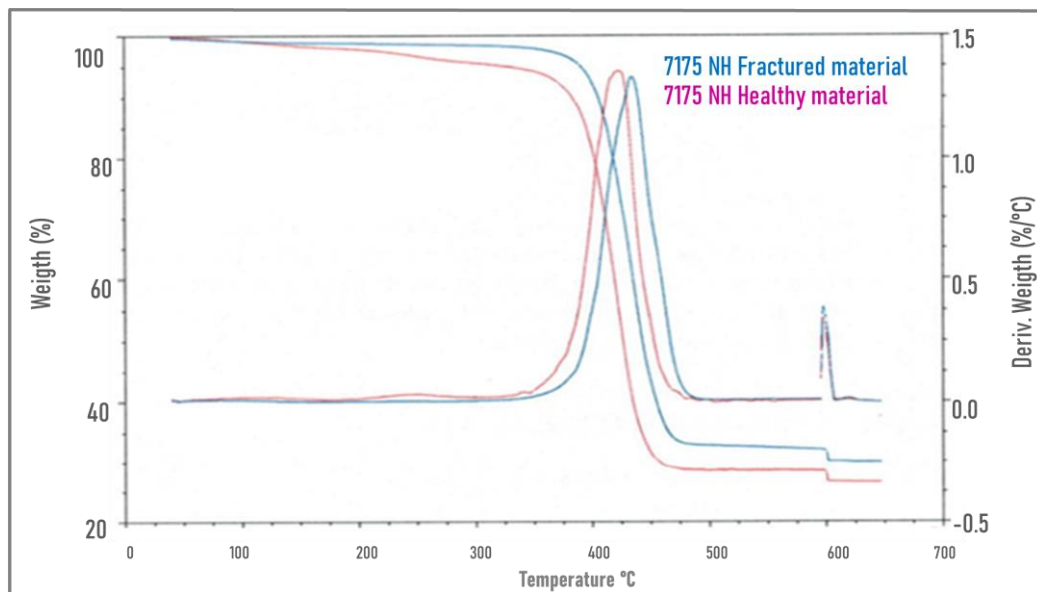


Figure 5. Comparative thermogram of a TGA of sample 7175 NH healthy material and fractured material.

Table 1. Results obtained in the TGA of the healthy material and fractured material.

Sample	40–300 °C (%)	300–600 °C (%)	600–650 °C (%)	Tmax (°C)	Waste (%)
Healthy material	1.28	66.58	1.87	434.13	29.84
Fractured material	4.40	66.99	1.95	423.14	26.42

Figure 5 shows a comparative thermogram of both materials in which it can be appreciated that the fractured material starts losing mass at low temperatures and is less stable in comparison to the healthy material. Displacement degradation on the curve maximum value shows a fracture at 423.14 °C versus the one obtained in the non-fractured sample of 434.13 °C, indicating that there is minor thermal stability in the fractured material.

3.4. Optical Microscopy

Images in Figure 6, obtained from optical microscopy, show the surface roughness of the fractured material (Figure 6b) in comparison to the healthy material (Figure 6a), which presents a regular surface. Figure 6c shows the fractured material at 40× with some cracking areas on the surface being visualized.

Additionally, in the failure zones with intentional fractures (Figure 7), some holes can be appreciated that suggests a different fracture mechanism. These holes could have previously existed exactly as shown in the tomography results or could have appeared during the fracture process (as a ductile fracture). In the end, in the failure zones, whether fractured or intentionally fractured materials, there are no signs of any type of contamination or fiber agglomeration that could generate a concentration of effects as a facilitator for failure.

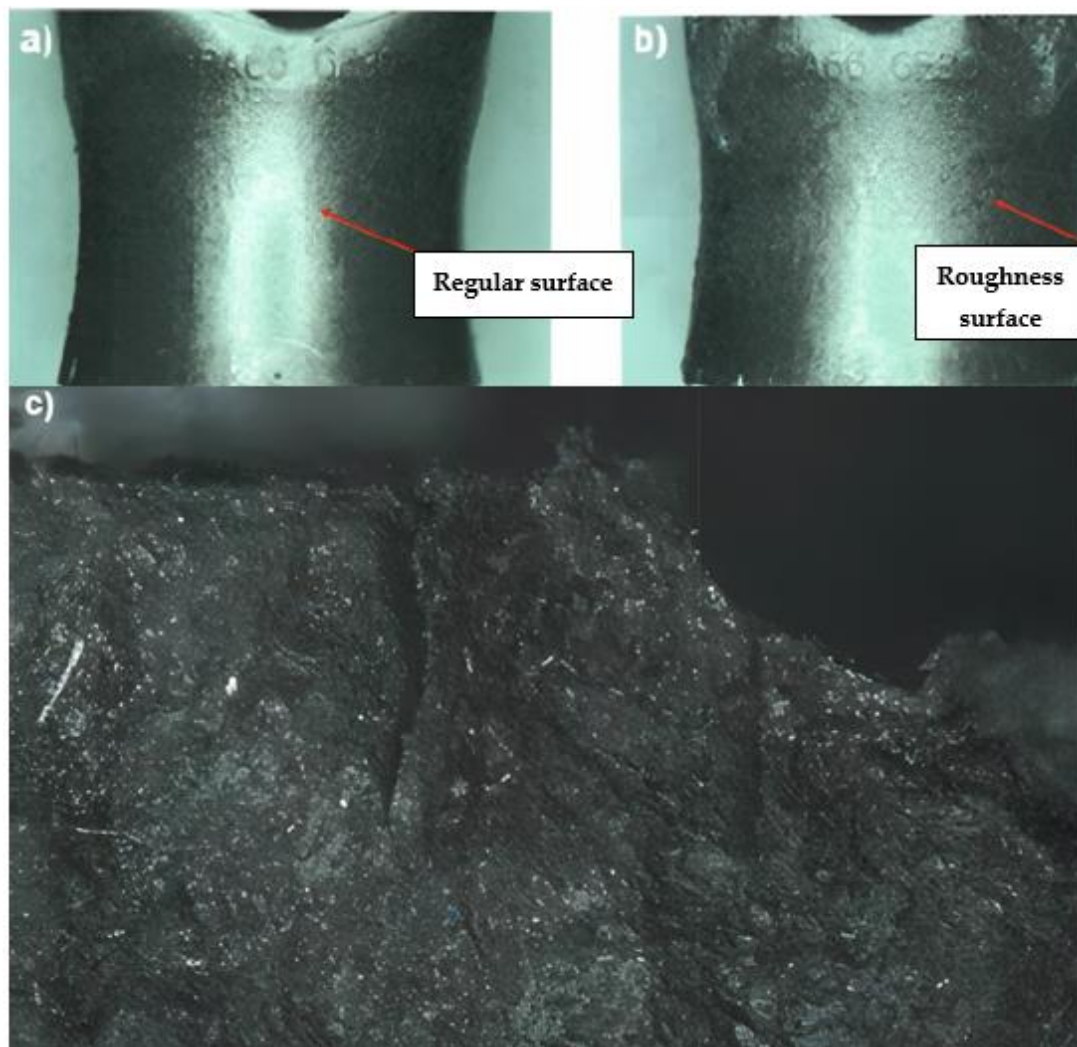


Figure 6. Micrograph of (a) 7175 NH healthy sample at $6.3\times$, 7175NH fractured sample of the left zone at (b) $6.3\times$, and (c) $40\times$.

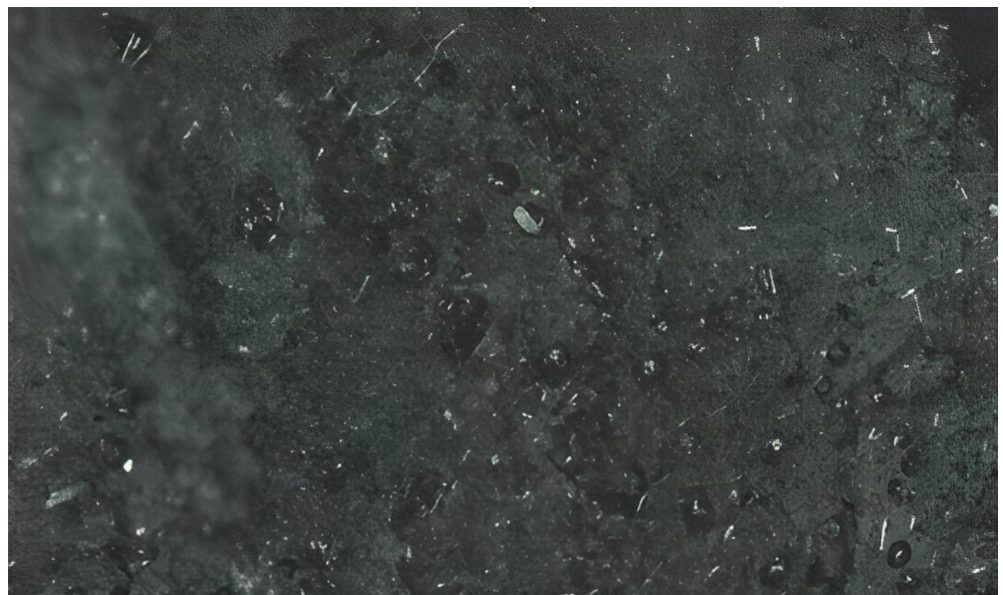


Figure 7. Micrograph of 7175 NH fractured sample, intentional upper area at $40\times$.

3.5. X-ray Tomography

Through tomography, a 3D image is created of the entire material volume, Figure 8 shows images that were obtained by X-ray tomography with some pores, however, zones with a higher pore concentration do not match to the one that presents with a fracture. Therefore, it is realistic to assume that these are not the main factor for the occurrence of failure. The results show a difference in composition percentages, primarily in volatile material content and less thermal stability in the fractured sample. On the other hand, it can be considered that the material can present a sort of fragility because of humidity. To improve comprehension of the material's performance, XCT has become an increasingly popular characterization method for deducing the mechanisms that cause deformation or failure in advanced materials on length scales ranging from tens of micrometers to several millimeters.

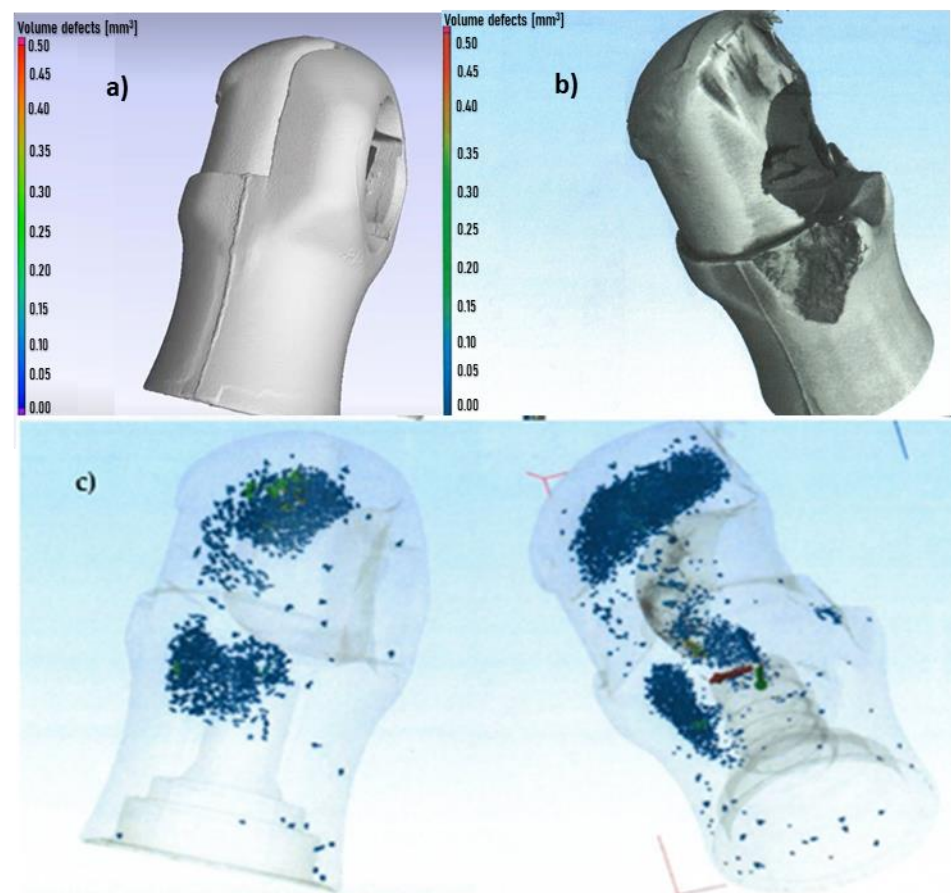


Figure 8. X-ray tomography of sample 7175N (a) healthy material, (b) fractured material, and (c) X-ray tomography comparative between the healthy sample (left side) and the fractured sample (right side).

Together, FTIR, DSC, and TGA results indicate that samples 7175 NH of the healthy and fractured materials are mainly related to nylon-6,6 with different fiberglass content of 29.84% and 26.42%, respectively (Figure 2). In addition, TGA results show less thermal stability, as well as an increase in volatile material percentage for the fractured sample 7175 NH.

Furthermore, images obtained from optical microscopy show a surface roughness in the fractured material with regard to that observed in the healthy material. In the same way, some differences in the surfaces generated in the fractures were spotted between the material with a fracture and the one intentionally fractured, which in turn suggests a different fracture mechanism. For the fracture sample, some fissures can be noticed, meanwhile, in the intentionally fractured material, there are some holes indicating a ductile

fracture instead [35]. These differences can derive from several causes, such as material mechanical integrity, variation in humidity content, crystallinity percentage, a previous degradation, or conditions under which the materials were fractured, such as temperature, humidity, or impact speed [36]

Finally, images that were obtained in the computerized X-ray tomography show pores in both samples, nevertheless, zones with a higher pore concentration do not match with the one where the fracture is located, therefore, it is logical to assume that these are not the main factor for failure occurrence. However, they still may be significant to the higher number of pores in the fractured sample rather than the healthy material.

4. Discussion

Nylon 6,6 is used where high mechanical strength, stiffness, good heat stability, or chemical resistance is required. It is used in textile and carpet fibers and molded parts. It has wide use in automotive applications; these include “under hood” parts such as the radiator end tanks, rocker covers, air intake manifolds, and oil pans, as well as numerous other structural parts, such as hinges and ball bearing cages. When considering whether nylon is suitable for a particular application, it is necessary before choosing the type of polyamide to consider its mechanical properties, water resistance, and ease of processing. For this particular part, a car rear door damper, nylon-6,6 30% glass fiber, has the best mechanical properties.

The results of this study indicate differences in composition percentages, mostly in volatile material content and low thermal stability for the fractured sample, which has been reported as evidence of thermal degradation for this type of material [7], although the presence of an external contamination factor that can be detected by FTIR spectroscopy is not excluded. Meanwhile, micrographs that show differences in fracture type can be considered a consequence of an increase in volatile materials content that, in the case of being merely humidity, could be a reason for provoking embrittlement in nylon contained in the fractured sample but this can be excluded if humidity content variation alters crystallinity variation percentage that can be formed in the sample [37] that do not happen as the DSc has reported. Another main reason that could provoke embrittlement in samples is a difference in crystallinity percentage in the processing conditions of the materials that can also generate a porosity variation inside them [38], but this can be excluded because the initial crystallinity percentages were similar in both situations. Similarly, there is the possibility that the resin that was used to shape them might be contaminated with organic materials of low molecular weight, and once they were processed, a compound fraction was liberated, creating a higher pore number. Even though it is possible that resin degrades during the processing and that volatile materials appear [7], either material could have been contaminated or exposed to conditions that promote degradation after the manufacturing process. All the above finding imply a change in the mechanical integrity of the fractured material but might not omit the fact that it could have been subjected to any type of impact or mechanical effort.

5. Conclusions

A study was carried out to know the causes for which a damping support 7175 NH of a car rear door made of nylon as its main element had mechanical failures. In the analyses of the results based on different characterization testing in a healthy material and a fractured sample, the following conclusions were reached:

1. It was determined by FTIR that there are no significant differences in the chemical bonds of both samples even though an increase in the peak is observed in the amorphous region and in the transition region, it was also identified that there is a gap in crystallinity degree in the healthy sample (29.84%) and the fractured sample (26.42%). TGA shows a lower thermal stability in the fractured sample, as well as an increase in volatile material amount.

2. In the FTIR analysis, characteristic functional groups of nylon-6,6, and fiberglass to a lesser extent, were found in both samples. Microscopy shows a surface roughness in the fractured sample that cannot be found in the healthy sample.
3. Computerized X-ray tomography displayed that if both samples show a pore zone, in the fractured sample there is a higher number of pores rather than the ones found in the healthy sample.
4. The change of these properties implies an alteration in the mechanical integrity of the fractured material.

Author Contributions: Conceptualization, J.C.-S., M.A.Z.-A., N.E.M.L., P.J.P.-K. and S.A.G.-L.; methodology, J.C.-S., N.E.M.L. and P.J.P.-K.; validation, J.C.-S. and S.A.G.-L. formal analysis J.C.-S. and G.V.-C.; investigation, J.C.-S., M.A.Z.-A., N.E.M.L., P.J.P.-K. and S.A.G.-L.; resources, J.C.-S.; data curation, J.C.-S., M.A.Z.-A., N.E.M.L., P.J.P.-K. and S.A.G.-L.; writing—original draft preparation, J.C.-S., M.A.Z.-A., N.E.M.L., P.J.P.-K. and S.A.G.-L.; writing—review and editing, J.C.-S., M.A.Z.-A., G.V.-C., N.E.M.L., P.J.P.-K. and S.A.G.-L. All authors have read and agreed to the published version of the manuscript.

Funding: This research received was funded by the National Vice Rector's Office for Research, Innovation and Business Incubator of UVM.

Data Availability Statement: The data presented in this study are available on request from the corresponding author. The raw data required to reproduce these findings cannot be shared at this time as the data also forms part of an ongoing study.

Acknowledgments: The authors would like to thank Isaura Itzel Acosta Sánchez for their technical contributions.

Conflicts of Interest: The authors declare no conflict of interest.

References

1. Kaliappan, S.; Balaji, V.; Raj, N.M.; Yatika, G.; Natrayan, L.; Shyam, D. Friction stir welding of nylon 6–6 thick plates using biochar colloidal nanoparticle. *Mater. Today Proc.* **2023**, in press. [\[CrossRef\]](#)
2. Rashed, K.; Kafi, A.; Simons, R.; Bateman, S. Fused filament fabrication of nylon 6/66 copolymer: Parametric study comparing full factorial and Taguchi design of experiments. *Rapid Prototyp. J.* **2022**, *28*, 1111–1128. [\[CrossRef\]](#)
3. Farbodi, M.; Mahdavi, B. Investigation of Morphology and Antibacterial Properties of Nylon 6, 6/PANI/ZnO Nanocomposite. *Int. J. New Chem.* **2022**, *9*, 282–290.
4. Khan, R.M.; Mushtaq, A. Effect of Reinforced Glass Fibre on the Mechanical Properties of Polyamide: Mechanical Properties of Polyamide. *Pak. J. Sci. Ind. Res. Ser. A Phys. Sci.* **2021**, *64*, 10–18. [\[CrossRef\]](#)
5. Sudhakar, M.; Priyadarshini, C.; Doble, M.; Murthy, P.S.; Venkatesan, R. Marine bacteria mediated degradation of nylon 66 and 6. *Int. Biodeterior. Biodegrad.* **2007**, *60*, 144–151. [\[CrossRef\]](#)
6. Nam, K.T.; Pant, H.R.; Jeong, J.W.; Pant, B.; Kim, B.I.; Kim, H.Y. Solvent degradation of nylon-6 and its effect on fiber morphology of electrospun mats. *Polym. Degrad. Stab.* **2011**, *96*, 1984–1988. [\[CrossRef\]](#)
7. Holland, B.J.; Hay, J.N. Thermal degradation of nylon polymers. *Polym. Int.* **2000**, *49*, 943–948. [\[CrossRef\]](#)
8. Polat, S.; Avci, A.; Ekrem, M. Fatigue behavior of composite to aluminum single lap joints reinforced with graphene doped nylon 66 nanofibers. *Compos. Struct.* **2018**, *194*, 624–632. [\[CrossRef\]](#)
9. Kim, D.K.; Lee, A.S.; Baek, B.K.; Song, K.H.; Hong, S.M.; Koo, C.M. PPE/nylon 66 blends with high mechanical toughness and flame retardancy. *Macromol. Res.* **2020**, *28*, 103–109. [\[CrossRef\]](#)
10. Zhang, M.; Gao, Q.; Yang, C.; Pang, L.; Wang, H.; Li, R.; Xing, Z.; Hu, J.; Wu, G. Preparation of antimicrobial MnO₄—doped nylon-66 fibers with excellent laundering durability. *Appl. Surf. Sci.* **2017**, *422*, 1067–1074. [\[CrossRef\]](#)
11. Deguchi, T.; Kakezawa, M.; Nishida, T. Nylon biodegradation by lignin-degrading fungi. *Appl. Environ. Microbiol.* **1997**, *63*, 329–331. [\[CrossRef\]](#)
12. Deguchi, T.; Kitaoka, Y.; Kakezawa, M.; Nishida, T. Purification and characterization of a nylon-degrading enzyme. *Appl. Environ. Microbiol.* **1998**, *64*, 1366–1371. [\[CrossRef\]](#)
13. Friedrich, J.; Zalar, P.; Mohorčič, M.; Klun, U.; Kržan, A. Ability of fungi to degrade synthetic polymer nylon-6. *Chemosphere* **2007**, *67*, 2089–2095. [\[CrossRef\]](#)
14. Klun, U.; Friedrich, J.; Kržan, A. Polyamide-6 fibre degradation by a lignolytic fungus. *Polym. Degrad. Stab.* **2003**, *79*, 99–104. [\[CrossRef\]](#)
15. Xie, K.; He, Y.; Cai, J.; Hu, W. Thermal conductivity of Nylon 46, Nylon 66 and Nylon 610 characterized by Flash DSC measurement. *Thermochim. Acta* **2020**, *683*, 178445. [\[CrossRef\]](#)

16. Sambale, A.; Kurkowski, M.; Stommel, M. Determination of moisture gradients in polyamide 6 using StepScan DSC. *Thermochim. Acta* **2019**, *672*, 150–156. [[CrossRef](#)]
17. Patti, A.; Acierno, S.; Nele, L.; Graziosi, L.; Acierno, D. Sustainable Basalt Fibers vs. Traditional Glass Fibers: Comparative Study on Thermal Properties and Flow Behavior of Polyamide 66-Based Composites. *ChemEngineering* **2022**, *6*, 86. [[CrossRef](#)]
18. Shinzawa, H.; Mizukado, J. Rheo-optical two-dimensional (2D) near-infrared (NIR) correlation spectroscopy for probing strain-induced molecular chain deformation of annealed and quenched Nylon 6 films. *J. Mol. Struct.* **2018**, *1158*, 271–276. [[CrossRef](#)]
19. Oshiro, M.; Takashima, K.; Furukawa, Y. Infrared Stark spectra for a Nylon 6 film. *Chem. Phys. Lett.* **2019**, *728*, 32–36. [[CrossRef](#)]
20. Černohorský, P.; Pisarenko, T.; Papež, N.; Sobola, D.; Ťálu, Š.; Částková, K.; Kaštyl, J.; Macků, R.; Škarvada, P.; Sedlák, P. Structure Tuning and Electrical Properties of Mixed PVDF and Nylon Nanofibers. *Materials* **2021**, *14*, 6096. [[CrossRef](#)]
21. Lim, J.V.; Bee, S.T.; Sin, L.T.; Ratnam, C.T.; Abdul Hamid, Z.A. Fabrication and Conductivity of Graphite Nanosheet/Nylon 610 Nanocomposites Using Graphite Nanosheets Treated with Supercritical Water at Different Temperatures. *Polymers* **2022**, *14*, 4660. [[CrossRef](#)]
22. de Lima, H.F.; Vaz, M.A.; da Costa, M.F.; Gomez, A.A.; de Oliveira, G.L. Creep behavior of in-service flexible flowline polyamide 11. *Polym. Test.* **2020**, *81*, 106205. [[CrossRef](#)]
23. Luna, C.B.B.; do Nascimento, E.P.; Siqueira, D.D.; Soares, B.G.; Agrawal, P.; de Mélo TJ, A.; Araújo, E.M. Tailoring Nylon 6/Acrylonitrile-Butadiene-Styrene Nanocomposites for Application against Electromagnetic Interference: Evaluation of the Mechanical, Thermal and Electrical Behavior, and the Electromagnetic Shielding Efficiency. *Int. J. Mol. Sci.* **2022**, *23*, 9020. [[CrossRef](#)]
24. Baranowski, T.; Dobrovolskij, D.; Dremel, K.; Hölzing, A.; Lohfink, G.; Schladitz, K.; Zabler, S. Local fiber orientation from X-ray region-of-interest computed tomography of large fiber reinforced composite components. *Compos. Sci. Technol.* **2019**, *183*, 107786. [[CrossRef](#)]
25. Liebrich, A.; Langowski, H.C.; Schreiber, R.; Pinzer, B.R. Porosity distribution in laser-sintered polymeric thin sheets as revealed by X-ray micro tomography. *Polym. Test.* **2019**, *76*, 286–297. [[CrossRef](#)]
26. Butenegro, J.A.; Bahrami, M.; Swolfs, Y.; Ivens, J.; Martínez, M.Á.; Abenojar, J. Novel Thermoplastic Composites Strengthened with Carbon Fiber-Reinforced Epoxy Composite Waste Rods: Development and Characterization. *Polymers* **2022**, *14*, 3951. [[CrossRef](#)]
27. *ASTM Designation D3418*; Standard Test Methods for Transition Temperatures and Enthalpies of Fusion and Crystallization of Polymers by Differential Scanning Calorimetry. ASTM International: West Conshohocken, PA, USA, 2015.
28. Movasaghi, Z.; Rehman, S.; ur Rehman, D.I. Fourier transform infrared (FTIR) spectroscopy of biological tissues. *Appl. Spectrosc. Rev.* **2008**, *43*, 134–179. [[CrossRef](#)]
29. Shueb, M.I.; Abd Manaf, M.E.; Ratnam, C.T.; Mohamad, N.; Mohamed, M. Enhancement of mechanical and electrical properties in graphene nanoplatelet modified nylon 66. *Malays. J. Compos. Sci. Manuf.* **2020**, *1*, 1–10. [[CrossRef](#)]
30. Linggawati, A.; Mohammad, A.W.; Ghazali, Z. Effect of electron beam irradiation on morphology and sieving characteristics of nylon-66 membranes. *Eur. Polym. J.* **2009**, *45*, 2797–2804. [[CrossRef](#)]
31. Cooper, S.J.; Coogan, M.; Everall, N.; Priestnall, I. A polarised μ -FTIR study on a model system for nylon 6 6: Implications for the nylon Brill structure. *Polymer* **2001**, *42*, 10119–10132. [[CrossRef](#)]
32. Xu, B.; Long, J.; Xu, G.; Yang, J.; Liang, Y.; Hu, J. Facile fabrication of superhydrophobic and superoleophilic glass-fiber fabric for water-in-oil emulsion separation. *Text. Res. J.* **2019**, *89*, 2674–2681. [[CrossRef](#)]
33. Krause, A.; Lange, A.; Erzin, M. *Plastics analysis guide: Chemical and instrumental methods.* Carl. Hanser Verlag. **1983**, 1983, 358.
34. Blaine, R.L. Thermal applications note. In *Polymer Heats of Fusion*; TA Instruments: New Castle, DE, USA, 2002.
35. Pawlak, A.; Galeski, A.; Rozanski, A. Cavitation during deformation of semicrystalline polymers. *Prog. Polym. Sci.* **2014**, *39*, 921–958. [[CrossRef](#)]
36. Flexman, E.A., Jr. Impact behavior of nylon-66 compositions: Ductile-brittle transitions. *Polym. Eng. Sci.* **1979**, *19*, 564–571. [[CrossRef](#)]
37. Hassan, A.; Rahman, N.A.; Yahya, R. Extrusion and injection-molding of glass fiber/MAPP/polypropylene: Effect of coupling agent on DSC, DMA, and mechanical properties. *J. Reinf. Plast. Compos.* **2011**, *30*, 1223–1232. [[CrossRef](#)]
38. Santulli, C.; Gil, R.G.; Long, A.C.; Clifford, M.J. Void content measurements in commingled E-glass/polypropylene composites using image analysis from optical micrographs. *Sci. Eng. Compos. Mater.* **2002**, *10*, 77–90. [[CrossRef](#)]

Disclaimer/Publisher's Note: The statements, opinions and data contained in all publications are solely those of the individual author(s) and contributor(s) and not of MDPI and/or the editor(s). MDPI and/or the editor(s) disclaim responsibility for any injury to people or property resulting from any ideas, methods, instructions or products referred to in the content.